AGU PUBLICATIONS

Water Resources Research

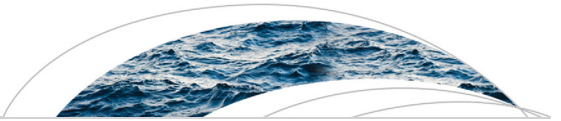

RESEARCH ARTICLE
10.1002/2017WR020410

Revisiting the horizontal redistribution of water in soils: Experiments and numerical modeling

L. Zhuang[1], S. M. Hassanizadeh[1,2], P. J. Kleingeld[1], and M.Th. van Genuchten[1,3]

[1]Department of Earth Sciences, Utrecht University, Utrecht, Netherlands, [2]Soil and Groundwater Systems, Deltares, Utrecht, Netherlands, [3]Department of Nuclear Engineering, Federal University of Rio de Janeiro, UFRJ, Rio de Janeiro, Brazil

Key Points:
- A series of experiments and related numerical simulations were carried out to study water redistribution processes in an unsaturated soil
- Two models, the standard Richards equation and an interfacial area model, were used to simulate the experiments
- The new formulation using the air-water interfacial area was able to simulate the experimental data

Correspondence to:
S. M. Hassanizadeh,
S.M.Hassanizadeh@uu.nl

Citation:
Zhuang, L., S. M. Hassanizadeh, P. J. Kleingeld, and M.T. van Genuchten (2017), Revisiting the horizontal redistribution of water in soils: Experiments and numerical modeling, *Water Resour. Res.*, *53*, 7576–7589, doi:10.1002/2017WR020410.

Received 13 JAN 2017
Accepted 1 AUG 2017
Accepted article online 3 AUG 2017
Published online 1 SEP 2017

Abstract A series of experiments and related numerical simulations were carried out to study one-dimensional water redistribution processes in an unsaturated soil. A long horizontal Plexiglas box was packed as homogenously as possible with sand. The sandbox was divided into two sections using a very thin metal plate, with one section initially fully saturated and the other section only partially saturated. Initial saturation in the dry section was set to 0.2, 0.4, or 0.6 in three different experiments. Redistribution between the wet and dry sections started as soon as the metal plate was removed. Changes in water saturation at various locations along the sandbox were measured as a function of time using a dual-energy gamma system. Also, air and water pressures were measured using two different kinds of tensiometers at various locations as a function of time. The saturation discontinuity was found to persist during the entire experiments, while observed water pressures were found to become continuous immediately after the experiments started. Two models, the standard Richards equation and an interfacial area model, were used to simulate the experiments. Both models showed some deviations between the simulated water pressures and the measured data at early times during redistribution. The standard model could only simulate the observed saturation distributions reasonably well for the experiment with the lowest initial water saturation in the dry section. The interfacial area model could reproduce observed saturation distributions of all three experiments, albeit by fitting one of the parameters in the surface area production term.

1. Introduction

Moisture redistribution is an important part of many near-surface and vadose zone hydrologic processes such as infiltration, root water uptake, evaporation, subsurface tile drainage, and recharge, including contaminant transport. Numerous studies over the years have focused on the basic processes of soil moisture redistribution and related capillary hysteresis processes, both experimentally [e.g., *Haines*, 1930; *Youngs*, 1958; *Biswas et al.*, 1966; *Staple*, 1966, 1969; *Gardner et al.*, 1970; *Vachaud and Thony*, 1971; *Peck*, 1971; *Talsma*, 1974; *Diment and Watson*, 1985; *van Dam et al.*, 1996; *Wang et al.*, 2003] as well as through numerical analyses [*Rubin*, 1967; *Dane and Wierenga*, 1975; *Youngs and Poulovassilis*, 1976; *Diment and Watson*, 1983; *Philip*, 1991; *van Duijn et al.*, 1995; *van Duijn and de Neef*, 1998; *Wang et al.*, 2004]. Most of these studies concerned redistribution after infiltration in vertical soil profiles or laboratory soil columns, while several experimental studies also investigated horizontal moisture redistribution and related hysteresis problems [*Feuring et al.*, 2014; *Kona*, 1997].

Various theoretical approaches have been used to account for the effects of hysteresis during moisture redistribution. Relevant models can be divided into two different approaches: (i) relatively conventional hysteresis models such as those used in the numerical studies cited above, with some also accounting for the effects of dynamic nonequilibrium flow [e.g., *Beliaev and Hassanizadeh*, 2001; *Beliaev and Schotting*, 2001] and (ii) an interfacial area model. We refer to the former approach as the standard (Richards) model. The latter approach introduces the specific fluid-fluid interfacial area, and corresponding governing equations, to account for hysteresis in the capillary pressure-saturation relationship [*Niessner and Hassanizadeh*, 2008; *Pop et al.*, 2009; *Zhuang et al.*, 2016]. Very few studies up to now have investigated the comparative ability of the two modeling approaches to simulate water redistribution experiments [*Zhuang et al.*, 2016].

In this paper, we provide results of a comprehensive experimental and numerical study of horizontal water redistribution in sand. We conducted a series of redistribution experiments in a custom-built horizontal sandbox (or flume) filled with a medium to coarse sand. The sandbox was divided into two sections by a very thin metal plate, with different initial water saturation in each section. The experimental results were simulated with both the standard model and the interfacial area model. In the following, we first describe the experimental setup and procedures. We then introduce the two modeling approaches, followed by a comparison of the experimental data with numerical simulation results.

2. Description of Experiments

2.1. Sand Properties

A medium to coarse sand (grain size 0.1–1 mm) taken from a riverbed in the Netherlands was used in the experiments. The sand had a mean particle diameter of 0.29 mm. Prior to use, the sand was rinsed with deionized water to remove clay particles, and then air dried. Unsaturated hydraulic properties of the sand were measured using a small laboratory setup as described in detail by *Zhuang et al.* [2017]. The saturated hydraulic conductivity was found to be 2.1×10^{-4} m/s, using the constant-head method [*Reynolds et al.*, 2002], while the average porosity of the sand sample was 0.37. Capillary pressure-saturation curves for primary drainage and main imbibition were measured with the hanging water column method [*Dane and Hopmans*, 2002]. Measured data in Figure 1a are shown by symbols. Simultaneously, unsaturated conductivities were measured directly for primary drainage and scanning imbibition using uniform gradient flow methods [e.g., *Dirksen and Matula*, 1994; *Weller et al.*, 2011]; the data are shown in Figure 1b. Observed data were analyzed in terms of the standard van Genuchten-Mualem equations [*Mualem*, 1976; *van Genuchten*, 1980] for water retention and the unsaturated hydraulic conductivity as follows:

$$p^c(S^w) = \frac{1}{\alpha}\left[S_e^{-1/m} - 1\right]^{1/n} \tag{1}$$

$$k^{rw}(S^w) = \omega(S_e)^l\left[1 - \left(1 - S_e^{1/m}\right)^m\right]^2 \tag{2}$$

$$S_e = \frac{S^w - S^w_{ir}}{1 - S^w_{ir} - S^a_r} \tag{3}$$

where $p^c(S^w)$ and $k^{rw}(S^w)$ are the capillary pressure and relative permeability curves, respectively, S^w_{ir}, S^a_r, S^w, and S_e are the irreducible water saturation, residual air saturation, water saturation, and effective water

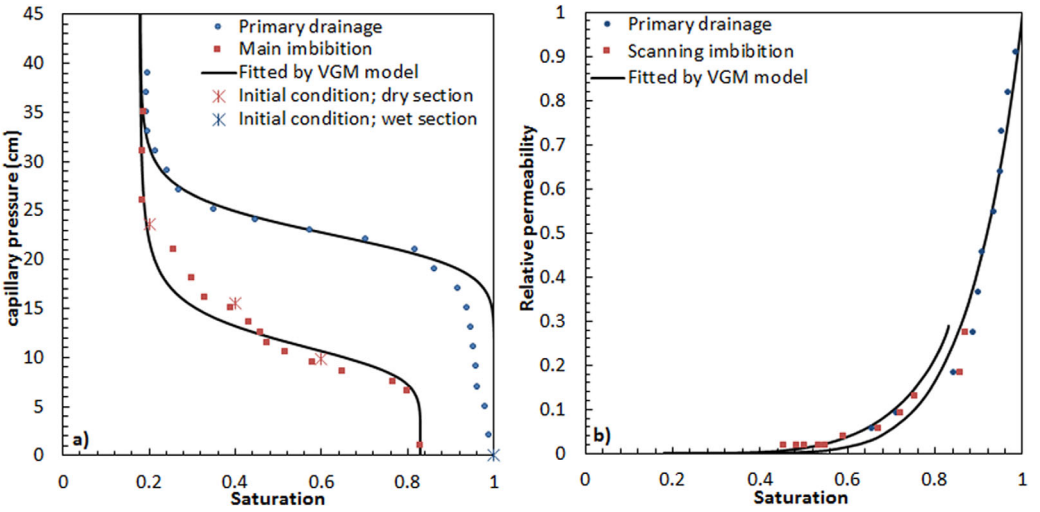

Figure 1. Measured and fitted (a) retention curves for primary drainage and main imbibition; (b) relative permeability curves for primary drainage and scanning imbibition.

Table 1. Measured Sand Properties and Fitted Hydraulic Parameter Values

Parameters		Unit	Value
Particle density, ρ^s		kg m^{-3}	2.55×10^3
Water density, ρ^w		kg m^{-3}	1×10^3
Water viscosity, μ^w		Pa s	1×10^{-3}
Saturated conductivity, K_S		m s^{-1}	2.1×10^{-4}
Intrinsic permeability, k		m^2	2.14×10^{-11}
Fitted hydraulic parameters in the van Genuchten-Mualem model			
Primary drainage	n		11.4
	α	Pa^{-1}	4.4×10^{-4}
	l		4.3
	$Sw\ ir$		0.18
Main imbibition	n		6.5
	α	Pa^{-1}	9.0×10^{-4}
	l		1.5
	ω		0.29
	$Sa\ r$		0.17

saturation, respectively, α, n, and l are the fitting parameters, and $m = 1 - 1/n$. The factor ω in equation (2) is introduced to account for the fact that the values of the unsaturated conductivity obtained for scanning imbibition do not reach the saturated conductivity value. The value of ω was set equal to the ratio between the largest measured value of the unsaturated conductivity and the saturated conductivity (the latter at full saturation). The fitted curves are shown as solid lines in Figures 1a and 1b. Fitted parameter values and measured sand properties are listed in Table 1.

2.2. Experimental Setup and Procedure

We designed and constructed a long Plexiglas sandbox with dimensions of 2 cm (width) $\times$ 2 cm (height) $\times$ 60 cm (length) to conduct the horizontal water redistribution experiments. A schematic of the sandbox is shown in Figure 2. The sandbox was divided into two sections: one being 20 cm long and the other 40 cm. They were separated by a very thin metal plate (0.1 mm in thickness). This construction made it possible to pack the two sections with sand at different initial saturations. The long section ($0 < x \leq 40$) was filled with fully saturated sand, while the short section ($-20 \leq x < 0$) was filled with drier sand. The two sections were tightly closed at the top using a thin Plexiglas lid (1 mm in thickness); while silicone tapes were used to keep the whole sandbox air-tight and prevent any evaporation of water. The water redistribution experiments started by removing the thin plate. Mechanical springs were used at the two ends of the sandbox in order to push the two sections toward each other as the thin plate was being removed. This ensured full contact between the dry and wet sands at all times.

Eleven water tensiometers and four air tensiometers (Rhizo Instruments, Wageningen, Netherlands) were installed along the sandbox, as shown in Figure 2. They allowed measurements of the water and air pressures every 1 min during the redistribution experiments. Locations of the tensiometers are given in Table 2. The water tensiometers were composed of a ceramic cup, 1 cm long and 4 mm in diameter, and a small pore pressure transducer. Air permeable but water impermeable plastic hollow fibers were used to connect the ceramic cups to vacuum in order to remove air from the tensiometers. The water tensiometers were saturated with deionized water prior to their use. The vacuum was always applied during the experiments to remove any air from the tubes between the ceramic cups and the transducers, so that they remained saturated. Teflon porous cups were used for the air-selective tensiometers. Very thin tubes, with a total volume of around 100 μL, were used to connect the hydrophobic porous cups with the transducers, while the joints between the thin tubes and the transducers were sealed with

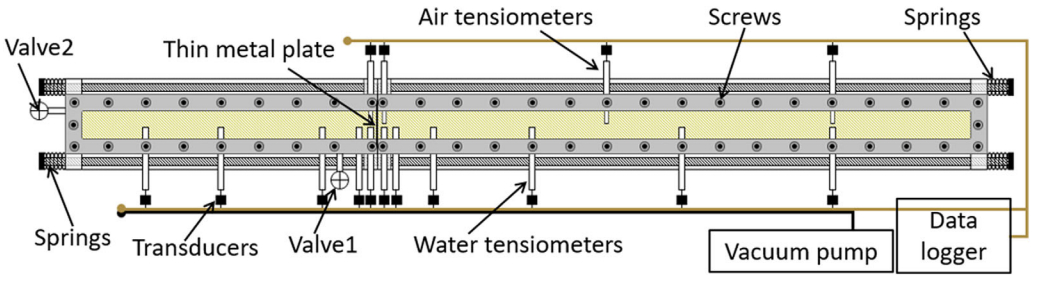

Figure 2. Schematic top view of horizontal sandbox before rotation; after rotation this became the side view. The upper and lower rows of tensiometers are for air and water, respectively.

Table 2. Coordinates of the Tensiometer Locations and Gamma Radiation Measurement Points

Devices	Sections	Locations (x in cm)
Water tensiometers	Dry	−0.5, −1.5, −3.5, −10, −15
	Wet	0.5, 1.5, 3.5, 10, 20, 30
Air tensiometers	Dry	−0.5
	Wet	0.5, 15, 30
Gamma radiation	Dry	−1, −2, −2.25, −2.5, −3, −4.5, −6.5, −8.5, −12.5, −18.5
	Wet	1, 2, 2.25, 2.5, 3, 4, 4.5, 6.5, 8.5, 10.5, 12.5, 14.5, 16.5, 18.5, 20.5, 22.5, 24.5, 26.5, 28.5, 30.5, 32.5, 34.5, 36.5, 38.5

thicker silicone tubes. The accuracy of water and air tensiometers was 0.5 cm. The water and air pressure transducers were connected to a CR1000 data logger (Campbell Scientific, Shepshed, UK) to allow continuous recording of the pressure values. A few water tensiometers were malfunctioned during the experiments. Their readings were not considered here.

A dual-energy gamma ray system was used to determine saturation and porosity values simultaneously at selected points along the sandbox. The accuracy of the saturation measurements for our soil system was about 0.5%. Coordinates of measured points are given in Table 2. Details of the saturation measurements using gamma radiation techniques are given in Appendix.

The sandbox was fixed onto a rotatable frame between the gamma source emitter and the detector. The top view is shown in Figure 2. After filling the box with sand (as explained below), the lid was firmly screwed down and the sandbox was rotated by 90° so that the lid was situated vertically. This allowed gamma measurements to be made through the lid. We used different procedures for filling the wet and dry sections of the sandbox. For the wet section, we first filled that part of the box with deionized and degassed water, after which clean air-dried sand was poured continuously and slowly into the water through a small funnel. The sand was regularly tapped and mixed using a small hair comb to prevent layering and promote the release of trapped gas. Sand for the dry section was first mixed with a certain amount of deionized and degassed water such that a large batch of sand with a prespecified saturation was obtained. Then, as for the wet section, the sand was packed into the long section of the sandbox, while again using a small comb to prevent layering.

Once both sections were filled, the two lids were fixed using screws and the whole sandbox was sealed. The system with its mounted tensiometers was next brought into position for the gamma radiation measurements. Moist air was pumped slowly into the dry section through Valve 1, while Valve 2 was kept open. This was continued overnight in order to ensure moisture equilibrium in the sandbox and to eliminate any potential for water evaporation during the experiments. A balloon filled with moist air was subsequently connected to Valve 2 (Figure 2), while Valve 1 was closed. The sandbox was then let to rest for several days, with the wet and dry sections still separated, in order to reach equilibrium. However, tensiometer and gamma radiation measurements were already collected during this period. The thin metallic plate was removed next to start the water redistribution process. As indicated earlier, the small gap between the dry and wet sections after removing the plate was eliminated by the action of springs. Moreover, silicon grease was applied around the joint to eliminate any leakage and/or water evaporation. The total weight of sand and water was recorded, before and after experiments, to verify that the overall water loss was negligible.

We performed three sets of experiments, with three different initial saturation values for the dry section: 0.2, 0.4, and 0.6. Table 3 summarizes these initial conditions of the experiments. All experiments were conducted in a constant-temperature room at 21 ± 0.5°C.

Table 3. Specifications of the Experiments

Experiments	Initial Saturation of the Dry Section	Initial Saturation of the Wet Section
I	0.2 ± 0.013	1.0 ± 0.015
II	0.4 ± 0.011	1.0 ± 0.012
III	0.6 ± 0.012	1.0 ± 0.012

3. 1-D Mathematical Models

In this section, we describe the two alternative mathematical formulations that were used to simulate the horizontal redistribution process. For both models, we assumed that the air pressure

was constant along the modeling domain. This assumption was supported by the air tensiometer measurements, which showed negligible spatial variations during the experiments.

3.1. Standard Model

Simulations with the standard model were carried out using the HYDRUS-1D finite element software package [*Šimůnek et al*., 2009]. The software uses the Richards equation for solving horizontal unsaturated flow in conjunction with hysteretic capillary pressure-saturation relationships as follows:

$$\varphi \frac{\partial S^w}{\partial t} + \frac{\partial}{\partial x}\left(-\frac{k^{rw}(S^w)k}{\mu^w}\left(\frac{\partial p^w}{\partial x}\right)\right) = 0 \tag{4}$$

$$-p^w = p^c(S^w) \tag{5}$$

where p^w denotes water pressure, p^c is the capillary pressure, t is the time, and x is the spatial coordinate. We note that dynamic capillarity effects are neglected when using equation (5).

When using HYDRUS-1D, every numerical node in the discretized domain can be assigned its own cluster of hysteresis scanning curves depending upon whether imbibition or drainage occurs. Two empirical approximations of capillary hysteresis, namely, *Kool and Parker* [1987] and *Lenhard and Parker* [1991], are included in HYDRUS-1D. In our study, we used the Lenhard-Parker approach to describe the scanning curves. In this approach, all scanning curves are scaled from the main imbibition or drainage curves by adjusting the residual air and irreducible water saturations (i.e., Sa_r and Sw_{ir}, respectively), but using the same values of α and n as the main imbibition or drainage curves. The fitted primary drainage curve was used for the wet section, while the fitted main imbibition curve and a reconstructed main drainage curve were used for the dry section. For the reconstructed main drainage curve, the value of α was assumed to be the same value as for primary drainage, while other parameters were given the same values as main imbibition. Measured average porosities were assigned to the dry and wet sections. This caused us to slight rescale the p^c-S^w curves.

For the HYDRUS-1D simulations, a grid size of 0.5 cm was used based on mesh independence tests. We assigned no-flow boundary conditions to both ends of the modeling domain, while water pressure and fluxes were assumed to be continuous at $x = 0$, where wet and dry sand touch. The initial saturation of the wet section was $S^w = 1$, while initial saturation of 0.2, 0.4, or 0.6 was assigned to the dry section.

3.2. Interfacial Area Model

The interfacial area model as used in this paper is described in detail by *Zhuang et al*. [2016]. The model assumes that capillary hysteresis can be accounted for indirectly by including a new state variable, the air-water specific interfacial area [*Hassanizadeh and Gray*, 1990, 1993]. The specific interfacial area, denoted by a^{wa}, is defined as the amount of air-water interfacial area per unit volume of the porous medium. The interfacial area model assumes that a^{wa} is a unique function of capillary pressure and saturation, which are now both considered to be independent variables. The set of hysteretic capillary pressure-saturation curves in this way is replaced by a single $p^c-S^w-a^{wa}$ surface. The projection of this surface onto the p^c-S^w plane would form all hysteretic capillary loops in the domain between the primary (or main) imbibition and drainage curves. A single $p^c-S^w-a^{wa}$ surface under quasi-static conditions has been reported to exist by several in both numerical studies [*Held and Celia*, 2001; *Joekar-Niasar et al*., 2008; *Joekar-Niasar and Hassanizadeh*, 2011, 2012] as well as experimentally [*Chen and Kibbey*, 2006; *Karadimitriou et al*., 2013, 2014].

Similar to traditional p^c-S^w curves, the $p^c-S^w-a^{wa}$ surface is a hydraulic property of a given soil. In principle, the $p^c-S^w-a^{wa}$ surface should be measured experimentally. However, since measurements of the specific interfacial area were not available, we constructed the surface in this study with the aid of p^c-S^w data points. Our approach is based on a method proposed by *Bradford and Leij* [1997], and described in detail by *Zhuang* [2017]. Despite its uncertainties and limitations [e.g., *Grant and Gerhard*, 2007], we found this indirect method to be sufficient for our modeling purposes, as a first-order approximation. For our study, it suffices that the projection of the $p^c-S^w-a^{wa}$ surface does reproduce the p^c-S^w curves in the p^c-S^w plane. The calculated $p^c-S^w-a^{wa}$ points were fitted by the following power function, proposed by *Joekar-Niasar and Hassanizadeh* [2012]:

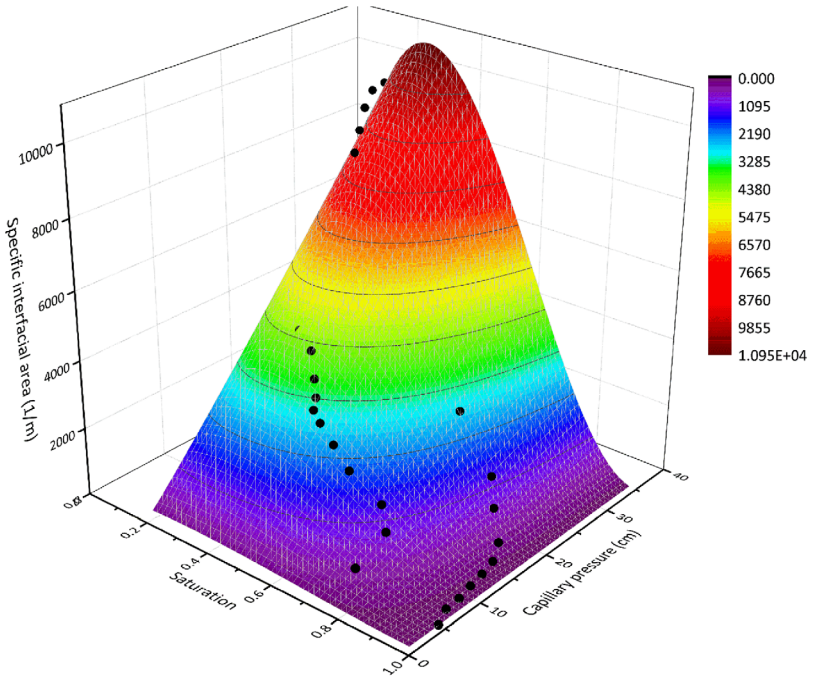

Figure 3. Three-dimensional $p^c-S^w-a^{wa}$ surface. The black symbols represent $p^c-S^w-a^{wa}$ points obtained using the method of *Bradford and Leij* [1997].

$$a^{wa}(S^w,p^c)=\gamma_1 S^w\ (1-S^w\ )^{\gamma_2}(p^c)^{\gamma_3} \tag{6}$$

where γ_1, γ_2, and γ_3 are the fitting parameters. The fitted $p^c-S^w-a^{wa}$ surface and its parameters are given in Figure 3 and Table 4, respectively. The black symbols in Figure 3 represent $p^c-S^w-a^{wa}$ points obtained using the method of *Bradford and Leij* [1997].

The interfacial area model introduces an evolution equation for the air-water specific interfacial area as follows [*Hassanizadeh*, 2015]:

$$\frac{\partial a^{wa}}{\partial t}+\frac{\partial(a^{wa}w^{wa})}{\partial x}=E^{wa} \tag{7}$$

where w^{wa} is the macroscopic flux of the specific interfacial area and E^{wa} is the net production rate of the specific interfacial area. Following *Zhuang* [2017], the latter is approximated by

$$E^{wa}=-L\frac{\partial a^{wa}}{\partial p^c}\frac{\partial S^w}{\partial t} \tag{8}$$

in which L is a material coefficient.

A review of the literature shows that the flux w^{wa} is very small [*Joekar-Niasar and Hassanizadeh*, 2011; *Karadimitriou et al.*, 2014]. Neglecting the corresponding term in equation (7) and using equation (8) leads then to

$$\frac{\partial a^{wa}}{\partial t}=-L\frac{\partial a^{wa}}{\partial p^c}\frac{\partial S^w}{\partial t} \tag{9}$$

The term E^{wa} accounts for the creation and destruction of interfaces during water redistribution. The material coefficient L is assumed to be different during drainage and imbibition, and given by [*Zhuang*, 2017]:

Table 4. Values of the Coefficients in Equation (6)

Parameter	Value	Standard Error
γ_1 [1/(Pa m)]	20.7	1.40
γ_2	2.0	0.15
γ_3	1.0	0.10
R^2	0.96	

$$L=\frac{L_{im}+L_{dr}}{2}+\frac{L_{im}-L_{dr}}{2}sign\left(\frac{\partial S^w}{\partial t}\right) \tag{10}$$

where L_{im} and L_{dr} denote the values of L for imbibition and drainage, respectively. These are optimized later using experimental data.

The interfacial area model also uses the Richards equation (4) to describe water flow. The set of equations to be solved hence are equations (4), (6), and (9). As before, the relative permeability is still assumed to be given by equation (2). Our measurements have shown that hysteresis in the relative permeability is negligible (see Figure 1b), in accordance with many previous studies [e.g., *Poulovassilis*, 1970; *Vachaud and Thony*, 1971; *Mualem*, 1986], which allows equation (2) to be written as a unique function of saturation.

The full set of equations for the interfacial area model was solved in terms of two primary variables: S^w and p^c. We used for this purpose the commercial package COMSOL Multiphysics 5.0 [*COMSOL*, 2014]. For the numerical solutions, we used a grid size of 0.1 cm, while residual errors were restricted to 10^{-8} based on mesh-independent tests. As initial condition for the various experiments, we used measured values of saturation and the capillary pressure. The solutions assumed continuity in the capillary pressure and water flux at $x = 0$. No-flow boundary conditions were assigned to the two ends of the domain.

4. Results and Discussion

4.1. Experiments

For Experiment I (initial saturation of 0.2 in the dry section), saturation values in the dry section ($x < 0$) increased markedly near the discontinuity within 1 h after redistribution started (see Figure 4), but then remained almost constant afterward. By comparison, saturation values in the wet section ($x > 0$) decreased over the entire wetted length almost evenly. This is due to the much higher unsaturated conductivities in the wet section, which required only very small water pressure gradients for any flow to occur. The entire redistribution process reached the equilibrium state after about one day. The saturation discontinuity at the contact interface ($x = 0$) persisted at all times.

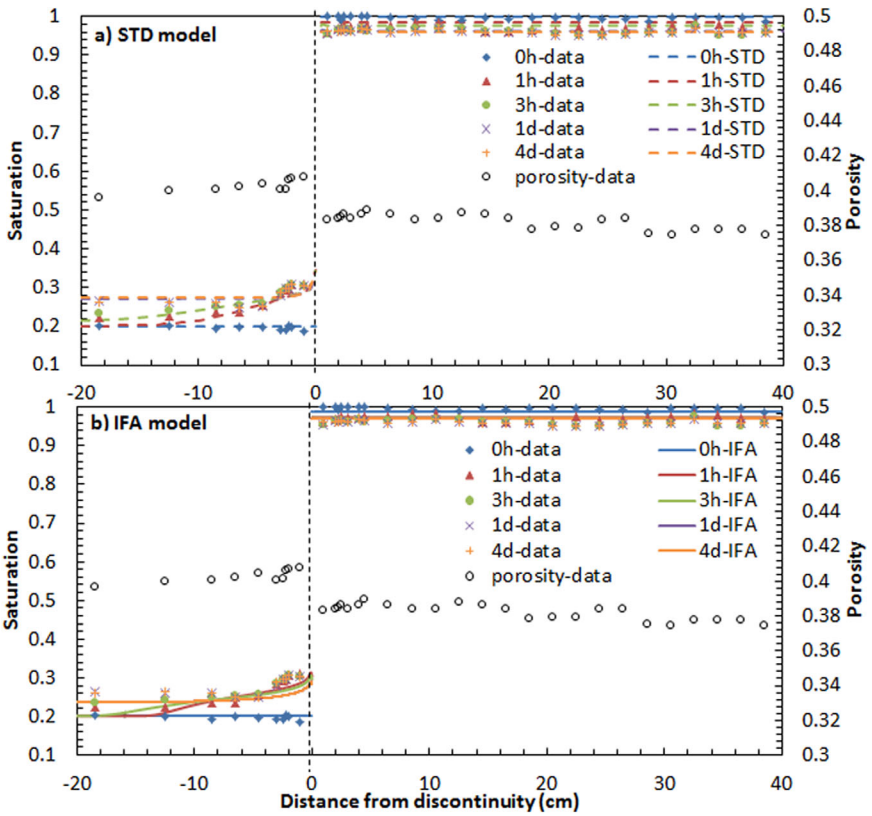

Figure 4. Measured porosity (open circles) and observed saturation profiles (other symbols) versus distance from the discontinuity for Experiment I, which had an initial saturation of 0.2 in the dry section. Also shown are simulated curves obtained with (a) the standard (STD) model (dashed lines) and (b) the interfacial area (IFA) model (solid lines).

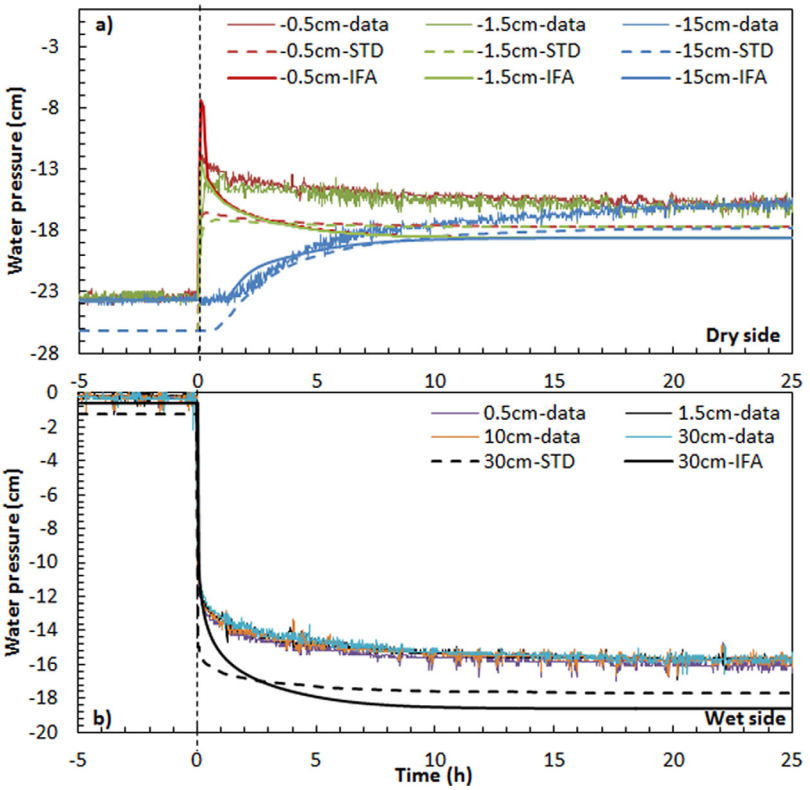

Figure 5. Measured water pressures versus time (thin lines) at several locations within (a) the dry and (b) the wet sections for Experiment I, which had an initial saturation of 0.2 in the dry section. Simulated curves obtained with the standard (STD) and interfacial area (IFA) models are shown as dashed and solid lines, respectively.

Measured water pressure heads as a function of time at several locations within the dry and wet sections of Experiment I are shown in Figures 5a and 5b, respectively. Thin colored lines with small fluctuations represent the pressure measurements. As can be seen in Figure 5a, at the point closest to the discontinuity in the dry section ($x = -0.5$ cm), the pressure increased at the start of the experiment, but then went down gradually to reach equilibrium. By comparison, the water pressure at the location farthest away from the discontinuity ($x = -15$ cm) increased only gradually during the redistribution process. Also, the dry section initially showed a large pressure head gradient, which disappeared gradually after about 1 day. However, water pressures in the wet section (Figure 5b) decreased monotonically and far more uniformly along the entire section. Pressure heads measured at -0.5 and 0.5 cm (close to the discontinuity) became almost the same after the initial spike in pressure at -0.5 cm dissipated. They subsequently both decreased gradually following similar patterns afterward. This implies that water pressures across the contact interface were continuous during the entire redistribution process.

For Experiments II and III, which had initial saturations of 0.4 and 0.6 in the dry section, respectively, measured saturation values changed monotonically in both the dry ($x < 0$) and wet sections ($x > 0$), as seen in Figures 6 and 8. For this reason, we show here only measured data close to the discontinuity ($-10 < x < 10$). For both experiments, the magnitude of the saturation discontinuity decreased compared to the initial value, but persisted during the entire redistribution. Measured water pressure heads at different locations for the two experiments (II and III) are shown in Figures 7 and 9. Pressure heads at the locations near the discontinuity in the dry section exhibited again short-lived peaks for both experiments, but now with smaller peaks as compared to Experiment I (which had an initial saturation of 0.2 in the dry section). Experiment III (having an initial saturation of 0.6) showed the smallest peak in the dry section after redistribution started.

While Experiment I showed considerable redistribution of moisture between the dry and wet sides, little redistribution had occurred in Experiments II and III when reaching equilibrium. This was actually expected

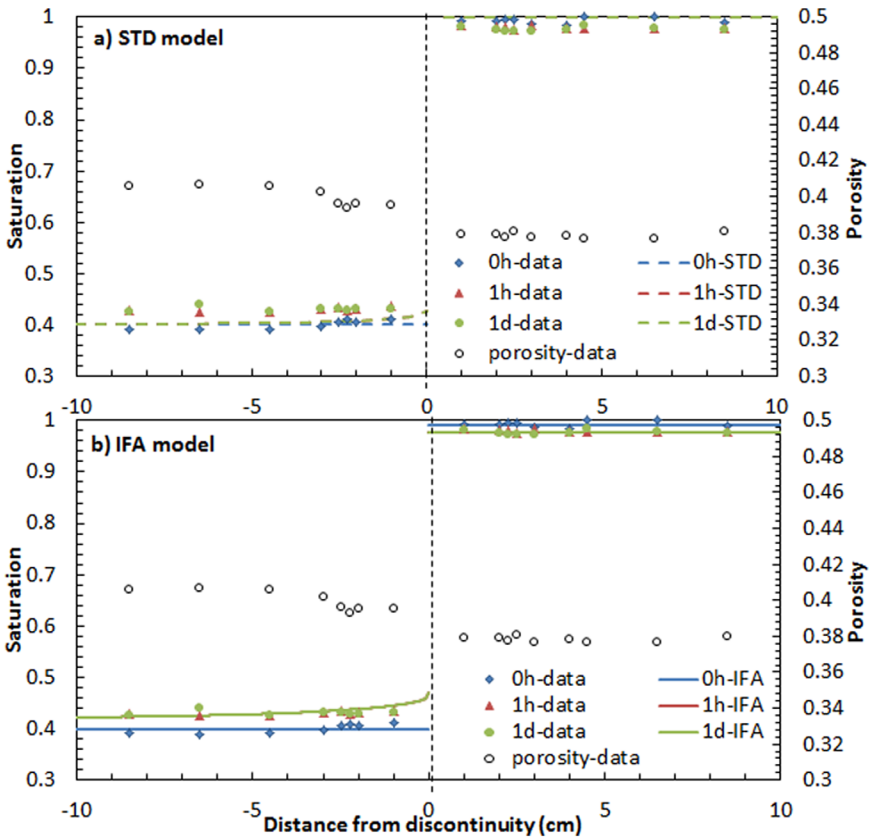

Figure 6. Measured porosities (open circles) and observed saturation profiles (other symbols) versus distance from the discontinuity for Experiment II, which had an initial saturation of 0.4 in the dry section. Also shown are simulated curves obtained with (a) the standard (STD) model (dashed lines) and (b) the interfacial area (IFA) model (solid lines).

from the initial water saturations in the two sections and considering the capillary pressure-saturation curves shown in Figure 1a. In that figure, we have indicated the initial conditions of the dry section in the three experiments by asterisk symbols, which are located nearly exactly on the main imbibition curve. The initial saturation of the wet section, on the other hand, was equal to unity for all three experiments (shown by a red asterisk on the primary drainage curve). Imbibition of the dry sections hence all followed more or less the main imbibition curve, while the wet section drained following the primary drainage curve. These processes should continue until the water pressures are the same in both sections. We can see from Figure 1a that this would have been achieved with very small reductions in saturation of the wet section, and only limited increases in saturation of the dry section in case of Experiments II and III, thus implying very little overall water redistribution. More significant water redistribution had to occur in case of Experiment I before pressure of the two sections would become equal. The exact pressures and saturation values at equilibrium, however, cannot be easily determined without numerical modeling. Obviously, the observed complete transient behavior of saturation and pressure in time, as well as their spatial distributions, can be determined only numerically.

4.2. Simulations

The three experiments were simulated using both the standard (STD) model (as programmed in HYDRUS-1D) and the interfacial area (IFA) model summarized earlier. For the simulations, using the standard model we assumed that initially the sand was in an imbibition state everywhere, consistent with the manner in which the sandbox had been packed. Initial conditions for the HYDRUS simulations were specified in terms of saturation values (not water pressure heads). For the interfacial area model simulations, we used the measured water saturations and pressure distributions as initial conditions. A single $p^c-S^w-a^{wa}$ surface was used for both sections. The values of L_{im} and L_{dr} in equation (10) were optimized based on measured

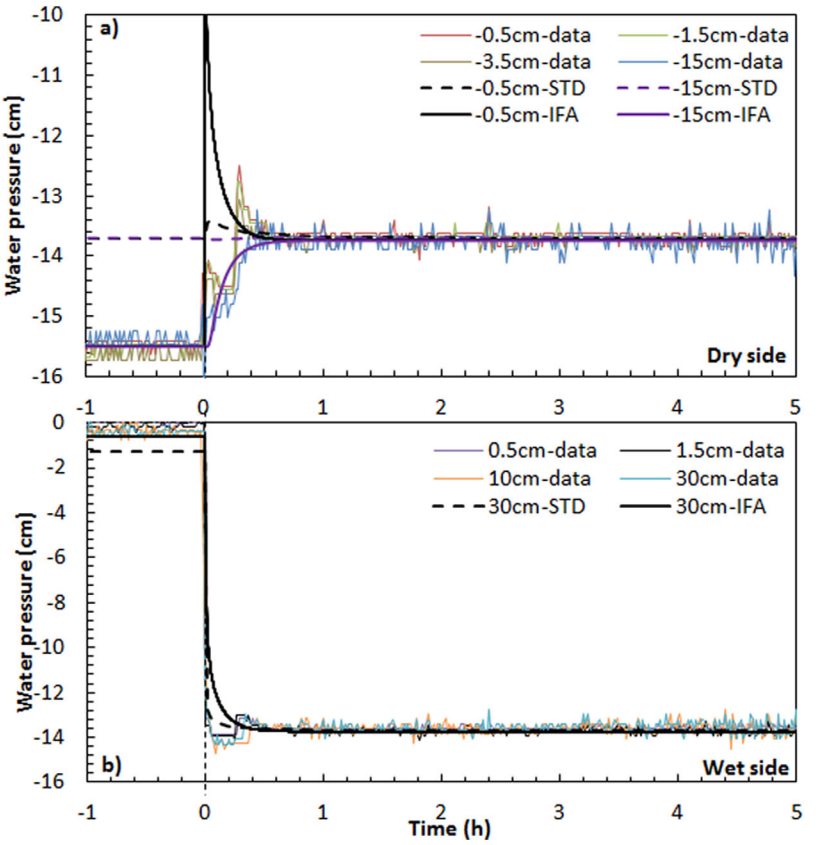

Figure 7. Measured water pressures versus time (thin lines) at several locations within (a) the dry and (b) the wet sections for Experiment II, which had an initial saturation of 0.4 in the dry section. Simulated curves obtained with the standard (STD) and interfacial area (IFA) models are shown as dashed and solid lines, respectively.

saturation and pressure data, producing the values shown in Table 5. Simulation results obtained with the standard (STD) model are shown as dashed lines in Figures 4–9, while solid lines represent results obtained with the interfacial area (IFA) model. Since water pressure heads at different locations in the wet section differed only slightly, simulated curves of the pressures versus time are shown for only one position.

As can be seen in Figure 4 for Experiment I, simulation results obtained with the standard and the interfacial area models both reproduced the measured saturation distributions reasonably well, provided we also adjusted the value of parameter l in equation (2). We found a value of -0.8 for both the interfacial area model and the standard model. For Experiments II and III, we used a value of 1.5 for l as obtained by fitting the relative permeability curve (see Table 1). Figure 5 shows that simulated water pressures obtained with both models still deviated slightly from the measurements.

Simulations of Experiments II and III (Figures 6–9) show that the standard model predicted only minimal redistribution of water. Little redistribution obtained with the standard model for Experiments II and III was probably due to the discrepancy between the measured retention data and the fitted van Genuchten curve for $0 < p^c < 17$ cm. Both models showed some deviations between the simulated water pressures and the measured data at early times of the redistribution processes. However, the interfacial area model captured the measured water pressure data at equilibrium better.

We note that either initial saturation or water pressure distributions can be specified as initial condition in the standard model. This led to an inconsistency in the initial saturations and water pressures (see Figures 5, 7 and 9). This discrepancy can be eliminated by adjusting the imbibition $p^c - S^w$ curve (which was measured independently and is shown in Figure 1), based on measured initial water saturations and

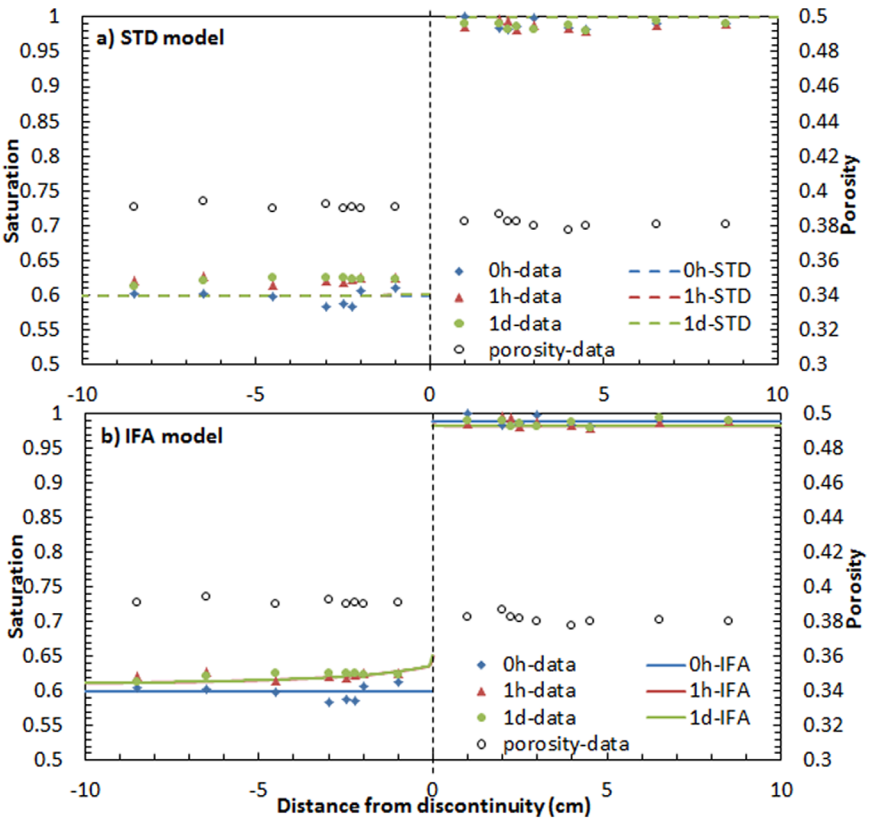

Figure 8. Measured porosities (open circles) and observed saturation profiles (other symbols) versus distance from the discontinuity for Experiment III, which had an initial saturation of 0.6 in the dry section. Also shown are simulated curves obtained with (a) the standard (STD) model (dashed lines) and (b) the interfacial area (IFA) model (solid lines).

pressures for each experiment. However, shifting the imbibition p^c-S^w curve for each experiment seemed unreasonable and nonphysical. By comparison, both the initial saturation and water pressure can be specified in the interfacial area model, thus allowing more consistency in the initial conditions.

As shown in Table 5, different values of L_{dr} were used for the dry and wet sections in the interfacial area model simulations, respectively. This can be explained by the fact that the coefficient L in principle depends on the two state variables S^w and a^{wa}. Its value hence may be different during different stages of wetting and drying. For our study, we selected different but constant values for each section. Indeed, micromodel studies [e.g., *Karadimitriou et al*., 2014] have shown that L is a material property and may depend on saturation. We emphasize that additional analyses and experiments are still needed to investigate the uncertain parameters in the interfacial area model.

We further note that the interfacial area model contains three parameters in the equation for $p^c-S^w-a^{wa}$ surface (i.e., γ_1, γ_2, and γ_3), which were determined based on measured $p^c-S^w-a^{wa}$ points. For the van Genuchten model, we need four parameters (i.e., α, n, $Sw\ ir$, and $Sa\ r$). In order to model the scanning curves in the van Genuchten retention equation, one needs to specify different $Sw\ ir$ or $Sa\ r$ values for each scanning curve, whereas for the interfacial area model no additional parameter is needed to model hysteresis. Instead one has to specify two parameters for the surface area production term, i.e., L_{im} and L_{dr}. The advantage of the standard model is that no fitting of parameter values for modeling transient data is needed. But for the interfacial area model, the parameters L_{im} and L_{dr} are chosen so that simulation results fit the transient data. Hence, to have a fair comparison of the models, additional transient experiments should be performed and simulated without changing the values of L_{im} and L_{dr}.

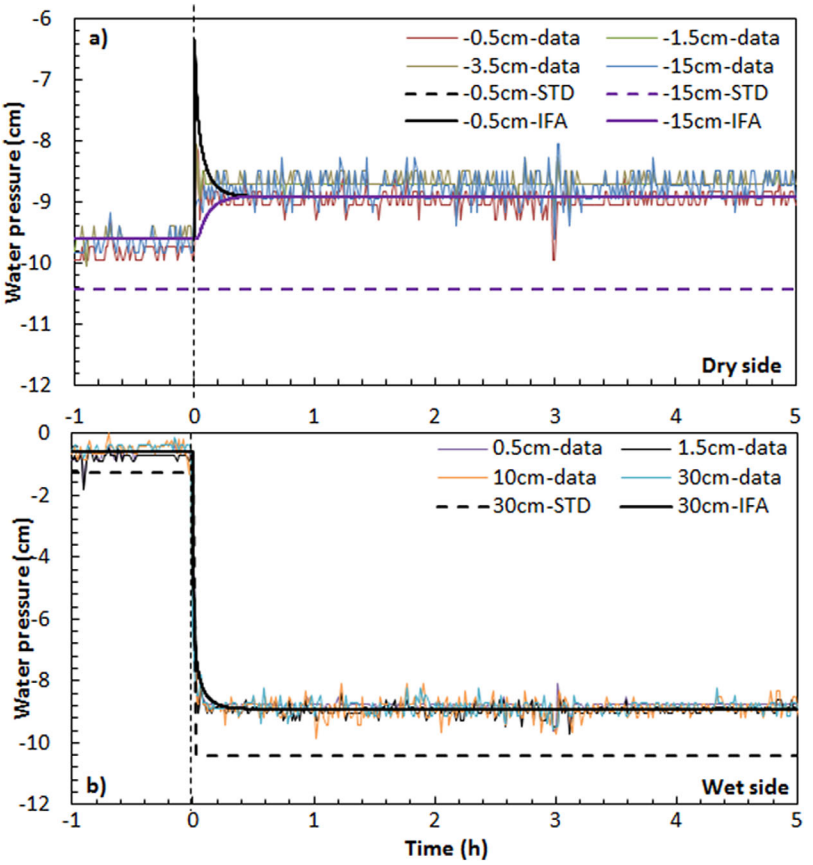

Figure 9. Measured water pressures versus time (thin lines) at several locations within (a) the dry and (b) wet sections for Experiment III, which had an initial saturation of 0.6 in the dry section. Simulated curves obtained with the standard (STD) and interfacial area (IFA) models are shown as dashed and solid lines, respectively.

5. Summary and Conclusions

In this study, we performed a series of well-defined horizontal water redistribution experiments in an unsaturated soil using a custom-built thin Plexiglas sandbox. The sandbox was filled with fully saturated sand in one section and partially saturated sand in the other section. We conducted three sets of experiments with different initial water saturations in the dry section (0.2, 0.4, and 0.6). Gamma transmission methods were used to measure water saturations at different locations along the sandbox, while water, and air tensiometers were installed at various positions to collect pressure data. As soon as a very thin metal plate separating the wet and dry sections was removed, the magnitude of the discontinuity in water saturation decreased, but persisted in all experiments. Water pressures near the contact interface were found to become continuous immediately after the experiments started. We observed that the degree of water redistribution decreased when the initial water saturation in the dry section was larger, i.e., for smaller differences in saturation between the wet and dry sections.

Two different models (the standard Richards equation and an interfacial area model) were employed to simulate the three sets of experiments. Both models showed some deviations between the simulated water pressures and the measured data at early times during redistribution. The standard model could simulate the water saturation distributions for the experiment having the lowest initial water saturation (about 0.2). However, contrary to observations, the standard model predicted almost no water redistribution for the other two experiments. The interfacial area model still could reproduce observed water saturation distributions for all three experiments, albeit by fitting the value of the coefficient L in area production term. We must point out that the

Table 5. Fitted Values of L_{im} and L_{dr} in the Interfacial Area Model

Dry Section		Wet Section
L_{im} (Pa)	L_{dr} (Pa)	L_{dr} (Pa)
9000	15,000	180,000

interfacial area model contains several adjustable parameters, which as such is a drawback but also could provide more flexibility in describing experimental data. Nevertheless, the interfacial area model is a more physically based approach for modeling capillary hysteresis in porous media.

Appendix: Simultaneous Measurement of Saturation and Porosity by Gamma System

Gamma radiation attenuation in an unsaturated soil sample can be described using Beer-Lambert's equation. Our gamma system consisted of ^{241}Am, with an energy peak of 59 keV, and ^{137}Cs, with an energy peak of 662 keV. Thus, two equations can be written for the measured attenuated intensities:

$$I^{Am}=I_0^{Am}\exp\left(-\mu_s l_s-\mu_w l_w\right) \quad \text{and} \quad I^{Cs}=I_0^{Cs}\exp\left(-\mu_s l_s-\mu_w l_w\right) \tag{11}$$

where I and I_0, with indices for the two sources, denote measured and corresponding reference intensities, respectively, μ_s and μ_w are the solid and water attenuation coefficients, respectively, and l_s and l_w denote the overall length of the solid and water phases along the path of the gamma-ray beam, respectively.

The diameter of the gamma-ray beam was 6 mm. Measured intensities, hence, were average values over the cross section of the beam and the soil thickness. The attenuation coefficients μ_s and μ_w for both ^{241}Am and ^{137}Cs were measured and calculated beforehand. Details of the calibration procedure information about the dual gamma ray system can be found in *Fritz* [2012]. The values of reference intensities I_0 for both ^{241}Am and ^{137}Cs were set equal to the measured intensities of the empty sandbox. At any given time and position, values of l_s and l_w could be calculated from measured intensities for ^{241}Am and ^{137}Cs using equation (11). Sand porosities (φ) and water saturations (S^w) consequently could be calculated at any given time and position from the following equations:

$$\varphi=\frac{l-l_s}{l} \quad \text{and} \quad S^w=\frac{l_w}{l-l_s} \tag{12}$$

respectively, and l is the total thickness of the soil sample (i.e., 2 cm, being the width of our sandbox).

Acknowledgments
We gratefully acknowledge Harm Gooren from Wageningen University, Thom Claessen, Sander Deelen, and Arjen de Waal from Utrecht University for technical support. The first author is supported by China Scholarship Council (201206380076). The second author received funding from the European Research Council under the European Union's Seventh Framework Programme (FP/2007–2013)/ERC grant agreement 341225. The second author would like to thank for the support received from the European Research Council (ERC) under the ERC Grant Agreement no. 341225. We would like to thank the Associate Editor and three anonymous reviewers for providing constructive comments to the manuscript. The data from this work can be accessed by contacting the corresponding author.

References

Beliaev, A. Y., and S. M. Hassanizadeh (2001), A theoretical model of hysteresis and dynamic effects in the capillary relation for two-phase flow in porous media, *Transp. Porous Media*, *43*(1), 487–510.

Beliaev, A. Y., and R. J. Schotting (2001), Analysis of a new model for unsaturated flow in porous media including hysteresis and dynamic effects, *Comput. Geosci.*, *5*(2), 345–368.

Biswas, T. D., D. R. Nielsen, and J. W. Biggar (1966), Redistribution of soil water after infiltration, *Water Resour. Res.*, *2*, 513–524.

Bradford, S. A., and F. J. Leij (1997), Estimating interfacial areas for multi-fluid soil systems, *J. Contam. Hydrol.*, *27*(1–2), 83–105, doi:10.1016/S0169-7722(96)00048-4.

Chen, L., and T. C. G. Kibbey (2006), Measurement of air-water interfacial area for multiple hysteretic drainage curves in an unsaturated fine sand, *Langmuir*, *22*(16), 6874–6880.

COMSOL (2014), COMSOL Multiphysics 5.0., COMSOL Inc., Burlington, Md.

Dane, J. H., and J. W. Hopmans (2002), Water retention and storage: Laboratory, in *Methods of Soil Analysis: Part 4 Physical Methods*, edited by J. H. Dane and G. Topp, *Methods of Soil Analysis: Part 4. Physical Methods*, pp. 675–720, Soil Sci. Soc. of Am., Madison, Wis., doi:10.2136/sssabookser5.4.c25.

Dane, J. H., and P. J. Wierenga (1975), Effect of hysteresis on the prediction of infiltration, redistribution and drainage of water in a layered soil, *J. Hydrol.*, *25*(514), 229–242.

Diment, G., and K. Watson (1983), Stability analysis of water movement in unsaturated porous materials: 2. Numerical studies, *Water Resour. Res.*, *19*, 1002–1010.

Diment, G., and K. Watson (1985), Stability analysis of water movement in unsaturated porous materials: 3. Experimental studies, *Water Resour. Res.*, *21*, 979–984.

Dirksen, C., and S. Matula (1994), Automatic atomized water spray system for soil hydraulic conductivity measurements, *Soil Sci. Soc. Am. J.*, *58*, 319–325, doi:10.2136/sssaj1994.03615995005800020009x.

Feuring, T., J. Braun, B. Linders, G. Bisch, S. M. Hassanizadeh, and J. Niessner (2014), Horizontal redistribution of two fluid phases in a porous medium: Experimental investigations, *Transp. Porous Media*, *105*, 503–515, doi:10.1007/s11242-014-0381-9.

Fritz, S. (2012), Experimental investigations of water infiltration into unsaturated soil—Analysis of dynamic capillarity effects, Master thesis, Stuttgart Univ., Germany. [Available at http://www.nupus.uni-stuttgart.de/07_Preprints_Publications/Preprints/Preprints-PDFs/Preprint_2012-7.pdf.]

Gardner, W. R., D. Hillel, and Y. Benyamini (1970), Post-irrigation movement soil water 1. redistribution, *Water Resour. Res.*, *6*, 851–861.

Grant, G. P., and J. I. Gerhard (2007), Simulating the dissolution of a complex dense nonaqueous phase liquid source zone: 1. Model to predict interfacial area, *Water Resour. Res.*, *43*, W12410, doi:10.1029/2007WR006038.

Haines, W. B. (1930), Studies in the physical properties of soil. V. The hysteresis effect in capillary properties, and the modes of moisture distribution associated therewith, *J. Agric. Sci.*, *20*(1), 97–116.

Hassanizadeh, S. M. (2015), Advanced theories of two-phase flow in porous media, in *Handbook of Porous Media*, 3rd ed., edited by K. Vafai, pp. 47–62, CRC Press, Boca Raton, Fla.
Hassanizadeh, S. M., and W. G. Gray (1990), Mechanics and thermodynamics of multiphase flow in porous media including interphase boundaries, *Adv. Water Resour.*, *13*(4), 169–186, doi:10.1016/0309-1708(90)90040-B.
Hassanizadeh, S. M., and W. G. Gray (1993), Thermodynamic basis of capillary-pressure in porous-media, *Water Resour. Res.*, *29*, 3389–3405.
Held, R. J., and M. A. Celia (2001), Modelling support of functional relationships between capillary pressure, saturation, interfacial area and common lines, *Adv. Water Resour.*, *24*, 325–343, doi:10.1016/S0309-1708(00)00060-9.
Joekar-Niasar, V., and S. M. Hassanizadeh (2011), Specific interfacial area: The missing state variable in two-phase flow equations?, *Water Resour. Res.*, *47*, W05513, doi:10.1029/2010WR009291.
Joekar-Niasar, V., and S. M. Hassanizadeh (2012), Uniqueness of specific interfacial area-capillary pressure-saturation relationship under non-equilibrium conditions in two-phase porous media flow, *Transp. Porous Media*, *94*, 465–486, doi:10.1007/s11242-012-9958-3.
Joekar-Niasar, V., S. M. Hassanizadeh, and A. Leijnse (2008), Insights into the relationships among capillary pressure, saturation, interfacial area and relative permeability using pore-network modeling, *Transp. Porous Media*, *74*, 201–219, doi:10.1007/s11242-007-9191-7.
Karadimitriou, N. K., M. Musterd, P. J. Kleingeld, M. T. Kreutzer, S. M. Hassanizadeh, and V. Joekar-Niasar (2013), On the fabrication of PDMS micromodels by rapid prototyping, and their use in two-phase flow studies, *Water Resour. Res.*, *49*, 2056–2067, doi:10.1002/wrcr.20196.
Karadimitriou, N. K., S. M. Hassanizadeh, V. Joekar-Niasar, and P. J. Kleingeld (2014), Micromodel study of two-phase flow under transient conditions: Quantifying effects of specific interfacial area, *Water Resour. Res.*, *50*, 8125–8140, doi:10.1002/2014WR015388.
Kona, S. (1997), Experimental investigation of horizontal redistribution of water in unsaturated porous media, MS thesis, University of Minnesota, Minn.
Kool, J. B., and J. C. Parker (1987), Development and evaluation of closed-form expressions for hysteretic soil hydraulic properties, *Water Resour. Res.*, *23*, 105–114.
Lenhard, R. J., and J. C. Parker (1991), Comparing simulated and experimental hysteretic two-phase transient fluid flow phenomena, *Water Resour. Res.*, *27*, 2113–2124.
Mualem, Y. (1976), A new model for predicting the hydraulic conductivity of unsaturated porous media, *Water Resour. Res.*, *12*, 513–522.
Mualem, Y. (1986), Hydraulic conductivity of unsaturated soils: Prediction and formulas, in *Methods Soil Analysis Part 1—Physical Mineralogical Methods*, 2nd ed., edited by A. Klute, pp. 799–823, ASA, Madison, Wis., doi:10.2136/sssabookser5.1.2ed.c31.
Niessner, J., and S. M. Hassanizadeh (2008), A model for two-phase flow in porous media including fluid-fluid interfacial area, *Water Resour. Res.*, *44*, W08439, doi:10.1029/2007WR006721.
Peck, A. J. (1971), Redistribution of soil water after infiltration, *Soil Res.*, *9*(2), 59–71.
Philip, J. R. (1991), Horizontal redistribution with capillary hysteresis, *Water Resour. Res.*, *27*, 1459–1469.
Pop, I. S., C. J. van Duijn, J. Niessner, and S. M. Hassanizadeh (2009), Horizontal redistribution of fluids in a porous medium: The role of interfacial area in modeling hysteresis, *Adv. Water Resour.*, *32*(3), 383–390, doi:10.1016/j.advwatres.2008.12.006.
Poulovassilis, A. (1970), The effect of the entrapped air on the hysteresis curves of a porous body and on its hydraulic conductivity, *Soil Sci.*, *109*(3), 154–162.
Reynolds, W. D., D. E. Elrick, E. G. Youngs, A. Amoozegar, H. W. G. Booltink, and J. Bouma (2002), Saturated and field-saturated water flow parameters, in *Methods of Soil Analysis: Part 4 Physical Methods*, edited by J. H. Dane and G. Topp, pp. 797–801, Soil Sci. Soc. of Am., Madison, Wis., doi:10.2136/sssabookser5.4.c30.
Rubin, J. (1967), Numerical method for analyzing hysteresis-affected post-infiltration redistribution of soil moisture, *Soil Sci. Soc. Am. Proc.*, *31*(1), 13–20, doi:10.2136/sssaj1967.03615995003100010009x.
Šimůnek, J., M. Sejna, H. Saito, M. Sakai, and M. T. van Genuchten (2009), The HYDRUS-1D software package for simulating the one-dimensional movement of water, heat and multiple solutes in variably-saturated media, Dep. Envir. Sci., Univ. of California, Riverside, Calif.
Staple, W. J. (1966), Infiltration and redistribution of water in vertical columns of loam soil, *Soil Sci. Soc. Am. J.*, *30*, 553, doi:10.2136/sssaj1966.03615995003000050010x.
Staple, W. J. (1969), Comparison of computed and measured moisture redistribution following infiltration, *Soil Sci. Soc. Am. J.*, *33*(6), 840–847.
Talsma, T. (1974), The effect of initial moisture content and infiltration quantity on redistribution of soil water, *Soil Res.*, *12*(1), 15–26.
Vachaud, G., and J. Thony (1971), Hysteresis during infiltration and redistribution in a soil column at different initial water contents, *Water Resour. Res.*, *7*, 111–127.
van Dam, J. C., J. H. M. Wösten, and A. Nemes (1996), Unsaturated soil water movement in hysteretic and water repellent field soils, *J. Hydrol.*, *184*(3–4), 153–173, doi:10.1016/0022-1694(95)02996-6.
van Duijn, C. J., and M. J. de Neef (1998), Similarity solution for capillary redistribution of two phases in a porous medium with a single discontinuity, *Adv. Water Resour.*, *21*(6), 451–461.
van Duijn, C. J., J. Molenaar, and M. J. de Neef (1995), The effect of capillary forces on immiscible two-phase flow in heterogeneous porous media, *Transp. Porous Media*, *21*(1), 71–93.
van Genuchten, M. T. (1980), A closed-form equation for predicting the hydraulic conductivity of unsaturated soils1, *Soil Sci. Soc. Am. J.*, *44*(5), 892–898.
Wang, Z., A. Tuli, and W. A. Jury (2003), Unstable flow during redistribution in homogeneous soil, *Vadose Zone J.*, *2*(1), 52–60, doi:10.2113/2.1.52.
Wang, Z., W. A. Jury, A. Tuli, and D.-J. Kim (2004), Unstable flow during redistribution, *Vadose Zone J.*, *3*(2), 549–559.
Weller, U., O. Ippisch, M. Köhne, and H.-J. Vogel (2011), Direct measurement of unsaturated conductivity including hydraulic nonequilibrium and hysteresis, *Vadose Zone J.*, *10*(2), 654–661, doi:10.2136/vzj2010.0074.
Youngs, E. G. (1958), Redistribution of moisture in porous materials after infiltration: 2, *Soil Sci.*, *86*(4), 202–207.
Youngs, E. G., and A. Poulovassilis (1976), The different forms of moisture profile development during the redistribution of soil water after infiltration, *Water Resour. Res.*, *12*, 1007–1012.
Zhuang, L. (2017), Advanced theories of water infiltration and redistribution in porous media; experimental studies and modeling, Ph.D. thesis, 170 pp., Utrecht University, Netherlands.
Zhuang, L., S. M. Hassanizadeh, M. T. van Genuchten, A. Leijnse, A. Raoof, and C. Qin (2016), Modeling of horizontal water redistribution in an unsaturated soil, *Vadose Zone J.*, *15*(3), 11, doi:10.2136/vzj2015.08.0109.
Zhuang, L., C. R. Bezerra Coelho, S. M. Hassanizadeh, and M. Th. van Genuchten (2017), Analysis of the hysteretic hydraulic properties of unsaturated soil, *Vadose Zone J.*, *16*(5), 9.